Predicting Sheet-Metal Part Form Deviation Using Discrete Inspection Points

(article starts on next page)

Available online at www.sciencedirect.com

ScienceDirect

Procedia CIRP 145 (2026) 129–134

www.elsevier.com/locate/procedia

19th CIRP Conference on Computer-Aided Tolerancing (CAT 2026)

Predicting Sheet-Metal Part Form Deviation Using Discrete Inspection Points

David Renborg[a,c,*], Peter Edholm[a], Maria Andrén[b], Kristina Wärmefjord[c], Lars Lindkvist[c], Rikard Söderberg[c]

[a] PE Geometry, Götaforsliden 13, 43134 Mölndal, Sweden
[b] Volvo Cars Corporation, Gunnar Engellaus v 8, 418 78 Göteborg
[c] Department of Industrial and Materials Science, Chalmers University of Technology, Hörsalsvägen 7A, 41296 Gothenburg, Sweden

* Corresponding author. *E-mail address:* david.renborg@pe-geometry.se

Abstract

In high-volume automotive production there is a need to describe the geometry of a part more accurately in early product-realization phases, when comprehensive measurement data are not yet available at scale, so that large-scale statistical variation analyses can be run quickly with simplified yet credible models. This paper proposes a method to predict part shape from sparse information by optimizing both the number and placement of inspection points subject to a defined accuracy threshold. Two production body-in-white parts, a compact inner d-pillar and a large outer fender, were 3D scanned with a Nikon H120 blue-laser high-precision scanner and compared against finite-element (FE) simulation models. The surface is reconstructed by combining the mesh and stiffness matrix of an FE-based material model implemented in a computer-aided tolerancing (CAT) software, RD&T, and the method is commissioned/validated against the scan. The study is experimental: a high-density scan is used as reference to evaluate how accurately sparse point constraints can reconstruct the full-field deformation. An error-driven greedy algorithm is used to iteratively select additional inspection points at locations where the current reconstruction deviates most from the scanned geometry, until the accuracy criterion is satisfied while minimizing model size and computation time.

Results indicate a correlation between the 3D-scanned geometry and the simulation-based reconstructions, demonstrating that the approach can reproduce part shape with reasonable precision for early-phase analyses. The method enables rapid simulations on large populations of parts with a reduced model that remains accurate enough to support decision-making in tolerancing and variation analysis. The reduced model is compatible with standard non-rigid Monte Carlo variation simulations in RD&T, enabling fast early-phase tolerance studies on large virtual populations of parts.

Peer-review under responsibility of the scientific committee of the 19th CIRP Conference on Computer-Aided Tolerancing (CAT 2026)

Keywords: computer-aided tolerancing; form prediction; 3D scanning; RD&T; finite-element modeling; greedy algorithm; variation analysis

1. Introduction

Geometrical variation in sheet-metal parts is a major contributor to quality issues in automotive body-in-white (BIW) production. Forming, springback, fixture variation and assembly operations introduce dimensional deviations that propagate through compliant assemblies and are typically addressed using CAT and early-phase variation simulation [1]. In these early phases, geometry descriptions must rely on sparse metrology information, since full-field optical scanning is costly and time-consuming, and the associated information loss is well documented [2, 3]. Instead, a limited number of inspection points, often defined on functional features or key surface regions, are used to characterize part deviation. While point-based descriptions are efficient and easy to integrate with simulation tools, they provide only partial information, making it difficult to predict the continuous surface shape between measured points or to capture more complex deformation modes.

This paper proposes a method for predicting sheet-metal part form from sparse measurement information using a finite-element stiffness representation. The approach reconstructs the surface by applying measured or simulated node displacements as boundary conditions to the FE stiffness matrix.

The work is conducted as an experimental evaluation in which a reference scan is used to quantify reconstruction ac-

2212-8271 © 2026 The Authors. Published by Elsevier B.V.

Peer-review under responsibility of the scientific committee of the 19th CIRP Conference on Computer-Aided Tolerancing (CAT 2026)
10.1016/j.procir.2026.03.127

curacy as the number and placement of discrete inspection constraints are varied.

The remainder of the paper is structured as follows. Section 2 reviews related work on sparse geometry representation, inspection planning and FE-based reconstruction. Section 3 describes the proposed methodology, including scanning, modelling and optimisation. The experimental study and calibration procedure are presented in Section 4. Results are given in Section 5, followed by discussion in Section 6. Section 7 concludes the paper.

2. Background and Related Work

Geometrical variation in sheet-metal parts has been extensively studied within the geometry assurance community, where non-rigid variation simulation, tolerance analysis and inspection planning all contribute to controlling variation throughout product realization. Geometry assurance frameworks describe how variation propagates through manufacturing and assembly and how digital models, tolerances and measurements can be used to predict downstream quality [4, 5]. Non-rigid variation simulation is now well established, enabled by FE-based sensitivity models such as the method of influence coefficients [1].

At the modelling level, the skin model and Skin Model Shapes (SMS) concepts extend nominal CAD by explicitly representing form deviations as discretised surface fields [6, 7]. More recently, data-driven approaches such as generative adversarial networks have been used to model statistical distributions of form defects from dense inspection data [8]. However, these methods rely on dense scanning or large measurement databases and do not address early-phase scenarios where only sparse inspection data are available.

Free-state behaviour and fixture-dependence pose additional challenges for compliant sheet-metal inspection. Virtual fixturing techniques use FE-based deformation models to transform measured free-state shapes into over-constrained inspection configurations [9, 10], for those cases measured forces need to be considered. These studies show that if the stiffness model is accurate and the boundary conditions are well defined, transformations between support states can be predicted with good precision. However, virtual fixturing assumes access to a full-field measurement of the part; it does not solve the inverse problem considered here, reconstructing a continuous deformation field when only a limited number of discrete inspection points is available.

Collectively, these studies highlight the importance of point placement but do not provide a physics-based mechanism to reconstruct the entire surface shape from sparse data.

The present work addresses precisely this gap. Unlike virtual fixture, which transforms existing full-field deviations between support conditions [9, 10], the proposed method reconstructs the full deformation field from only a sparse set of inspection-point deviations. Unlike inspection point-reduction methods, which quantify information loss or identify redundant points within an existing inspection plan [2], the proposed method actively expands the constraint set using the current reconstruction error. Finally, unlike SMS- or machine-learning-based form-defect models [6, 7] and data-driven form-defect models trained on dense measurement data [8], the proposed method does not require a defect basis or training database; the deformation field is obtained directly from the calibrated FE stiffness representation in RD&T.

3. Methodology

The proposed method described in this section is general and applicable to a wide range of compliant sheet-metal components, and no part-specific tuning is introduced.

Terminology: In the reconstruction, selected mesh nodes are treated as prescribed-displacement constraint nodes. The term "supports" is reserved for the physical spherical rests used during scanning.

3.1. Overview of the workflow

Figure 1 summarizes the proposed methodology, and Figure 2 details the adaptive constraint-node selection used in Step 3. First, a high-density reference scan is acquired on three physical supports and aligned to the nominal CAD geometry using the selected locating scheme. Second, a compliant FE model of the nominal geometry is established in RD&T, providing the mesh topology and global stiffness matrix K. Third, the aligned scan is mapped to the FE mesh as nodal deviation offsets, defining the reference deformation field u_{scan}. Reconstruction is then initiated from datum-related constraint nodes only. For the current active constraint set, the compliant solver computes a full-field deformation u_{rec}, compares it with the reference field, and iteratively expands the constraint set using the adaptive procedure described in Section 3.5 . Convergence is monitored using RMS and maximum absolute deviation, and the final outputs are a reduced constraint-node set and a full-field reconstructed geometry.

3.2. Data acquisition and 3D scanning

The parts were scanned using a Nikon H120 blue-laser scanner. Each part was placed on three spherical supports, providing a well-defined and repeatable near free-state condition while avoiding over-constraint during measurement. This setup is commonly used for compliant sheet-metal inspection, where fixture-induced deformation could mask the natural forming and springback behavior [10].

A high-density point cloud was generated and triangulated into an STL mesh. The STL was aligned to the nominal CAD geometry using the parts 3-2-1 locating scheme. This alignment procedure was kept identical for both components to ensure methodological consistency.

The aligned STL is then used as reference data for mapping scan deviations to the FE mesh and for evaluating reconstruction accuracy. The scan is used only as reference for evaluating reconstruction accuracy and for offline point-set identification; subsequent use requires only the selected discrete inspection-point deviations.

3.3. Finite-element model setup

Although the parts can differ substantially in size, curvature and stiffness distribution, the FE models were constructed using the

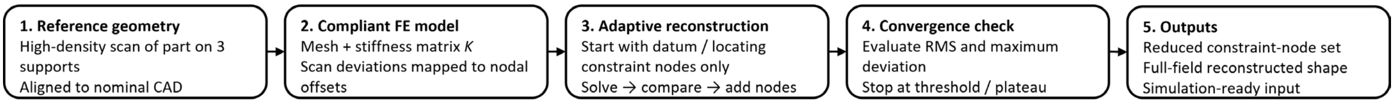

Fig. 1: Overview of the proposed methodology. A reference deviation field is obtained from the aligned scan and mapped to the compliant FE model. Starting from datum-related constraint nodes, the model reconstructs the full-field part shape iteratively, evaluates convergence, and outputs a reduced constraint-node set together with the reconstructed geometry. The adaptive node-selection procedure used in Step 3 is detailed in Fig. 2.

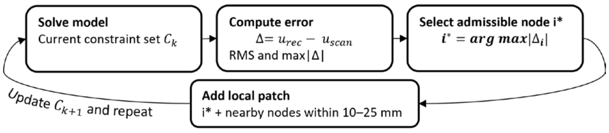

Fig. 2: Adaptive constraint-node selection in the compliant model. For the current constraint set C_k, the part shape is reconstructed and compared with the reference deviation field. The admissible node with the maximum absolute reconstruction error is selected, a local neighborhood patch is added, and the constraint set is updated until the convergence criterion is satisfied.

same modeling principles and similar mesh densities to ensure comparability. The shell elements were assigned the nominal sheet-metal thickness for each part.

3.4. Shape reconstruction from sparse inspection points

The reference scan is used to define a target deformation field relative to the nominal geometry. For each node i, the deviation of the scan from the nominal surface is stored as an offset value u_i^{scan}.

To reconstruct the shape from sparse information, only a subset of these inspection entities is activated, corresponding to constraint nodes in the FE model. The compliant solver combines the stiffness matrix with the active nodal displacements to compute a deformation field $\mathbf{u}_{\text{rec}}$ over the entire mesh, effectively predicting how the part would deform if only the sparse constraint nodes were known.

The quality of the reconstruction is evaluated by comparing the reconstructed deformation field $\mathbf{u}_{\text{rec}}$ with the reference field $\mathbf{u}_{\text{scan}}$ obtained from the imported scan offsets. For node i, the reconstruction error is defined as

$$\Delta_i = u_i^{\text{rec}} - u_i^{\text{scan}}. \tag{1}$$

From these nodal errors the root mean square (RMS) is computed, defined as:

$$\text{RMS} = \sqrt{\frac{1}{N}\sum_i \Delta_i^2} \tag{2}$$

where N is the number of nodes in the mesh.

In addition, the maximum absolute deviation $\max_i |\Delta_i|$ is monitored to identify the location where the reconstruction currently deviates most from the reference scan. These error measures are used both to assess the final reconstruction quality and to guide the adaptive constraint-node selection described in the next subsection. These quantities correspond to the error-evaluation and convergence steps shown in Fig. 1 and form the basis of the adaptive constraint-node selection shown in Fig. 2.

3.5. Adaptive greedy constraint-node selection

Reconstruction accuracy depends strongly on which nodes are activated as constraint nodes in the compliant model. The importance of constraint node placement for deformation stability and inspection sensitivity in sheet-metal parts is well documented in non-rigid variation simulation and fixture-layout research [11, 12]. Rather than selecting constraint nodes manually or using a predefined pattern, an adaptive greedy algorithm is employed to iteratively expand the constraint set based on reconstruction error.

In each iteration, the reconstructed deformation field is evaluated against the reference scan, and the nodes exhibiting the largest deviation are identified as candidates for new constraint nodes. Candidate nodes are then filtered to exclude nodes located on sharp edges or tight radii, since these regions exhibit rapidly varying surface normals and are more sensitive to local geometric discretization. The admissible set is therefore restricted to smoother surface regions with sufficient spacing from already active constraints. Similar geometric considerations have previously been shown to be important in both virtual fixture and inspection planning of compliant parts [2, 10].

From this admissible set, the node i^* with maximum $|\Delta_i|$ is activated as a constraint. To improve numerical stability, a small local constraint patch is added by activating n_{neigh} additional neighbor nodes within a distance band $10\,\text{mm} \leq \|x_j - x_i^*\| \leq 25\,\text{mm}$, which increases the constrained local area without becoming non-local.

The algorithm proceeds incrementally, expanding the constraint set until either a predefined threshold is satisfied or the reconstruction error reaches a stable plateau. Because the RMS curve may exhibit small iteration-to-iteration fluctuations, a stable plateau is identified when the range of RMS values over the last three iterations satisfies $max(RMS_{k-2:k}) - min(RMS_{k-2:k}) <$ 0.02mm. In the present study, a strict safeguard threshold of 0.05 mm is defined for the maximum absolute deviation. If this threshold is not reached within the iteration limit, convergence is instead assessed from the stabilization of the RMS metric. To reduce the influence of residual fluctuations, final RMS values are reported as the average over the last three iterations.

The same greedy selection strategy is applied to all test parts without geometry-specific tuning. Differences in convergence behaviour and achievable accuracy therefore reflect inherent differences in part size, stiffness distribution, and dominant deformation modes, rather than changes in algorithm parameters.

4. Experimental Studies

The experimental evaluation of the proposed method was conducted using two production BIW components (Fig. 3): an inner d-pillar and a front fender. Both parts were available as physical components together with their corresponding nominal CAD geometries, enabling direct comparison between measured and reconstructed shapes.

The data acquisition, alignment, finite-element modeling and reconstruction procedures defined in section 3 were applied to both components. For each part, a compliant finite-element representation based on the nominal geometry was imported into the CAT software RD&T together with its corresponding stiffness matrix. The aligned scan data were converted into inspection point information by assigning nodal deviation offsets to the finite-element mesh.

For each component, an initial reference configuration was evaluated in which only the locating features were activated as constraint nodes. This datum-only configuration serves as a baseline for assessing reconstruction performance and for verifying consistency in the compliant stiffness representation, scan-to-mesh node mapping, and the interpretation of prescribed displacement constraints prior to sparse reconstruction.

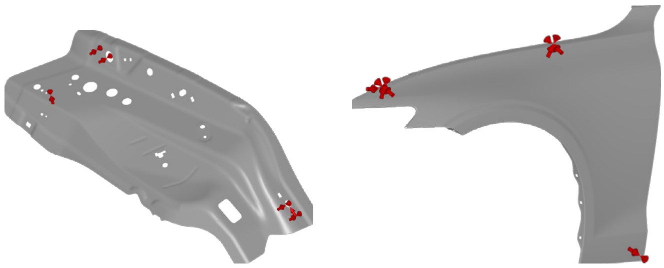

(a) Inner d-pillar (b) Front fender

Fig. 3: Test parts with datum only configuration

Starting from the datum-only configuration, reconstruction experiments were carried out using the adaptive greedy constraint node selection strategy described in Section 3.5. Additional constraint nodes were activated iteratively while previously selected constraint nodes remained active.

To study the influence of the number of neighbors added per iteration, two additional configurations were evaluated, in which three and four neighboring constraint nodes were added instead of two. In all cases the algorithm starts from the same datum-only initial configuration and uses identical stopping criteria.

Convergence time is defined here as the wall-clock runtime of the iterative reconstruction loop, measured from the initial datum-only reconstruction to the final iteration satisfying the stopping criterion defined in Section 3.5. The reported runtimes are indicative for the current research implementation and exclude preprocessing steps such as scan alignment, mesh generation, and scan-to-mesh mapping. Since the implementation has not been specifically optimized for computational efficiency, these values should be interpreted as indicative runtimes rather than benchmark measurements.

Reconstruction accuracy was evaluated by comparing the reconstructed deformation field with the reference scan using global error measures, including RMS deviation and maximum node-wise deviation. For each reconstruction run, error metrics were recorded as a function of iteration number and number of active constraint nodes. To reduce the influence of iteration-level fluctuations, final RMS values were computed as the average over the last three iterations of each run.

The recorded error metrics and the spatial distribution of selected constraint nodes form the basis for the analysis presented in section 5, where convergence behavior and differences between the two components are examined.

5. Results

This section presents the reconstruction results for both scanned parts. The d-pillar is analyzed first, followed by the fender. The main focus is on the configuration where the 2-neighbor setting is used, i.e., the peak-error node plus two neighbors are activated per iteration (three new constraint nodes per iteration).

5.1. Convergence behavior for the two-neighbor setting

The baseline reconstruction provides a RMS of 0.628 mm and the maximum absolute deviation is 2.27 mm.

When the greedy algorithm is run with a peak-error node plus two neighboring nodes added per iteration (i.e., three new constraint nodes per iteration in total), the set of constraint nodes on the primary datum surface is gradually expanded. Over 45 iterations, 135 additional constraint nodes are introduced, transforming the original 3–2–1 system into an N–2–1 system with 141 locators. The RMS deviation decreases overall as new constraints are added. Averaged over the final three iterations to reduce the influence of small fluctuations, the RMS converges to 0.224 mm. The largest improvement occurs during the first 15–20 iterations, after which the RMS curve flattens. Figure 4 illustrates the evolution of RMS deviation for the d-pillar as a function of iteration number. The corresponding iterative reconstruction required approximately 30 min of wall-clock time.

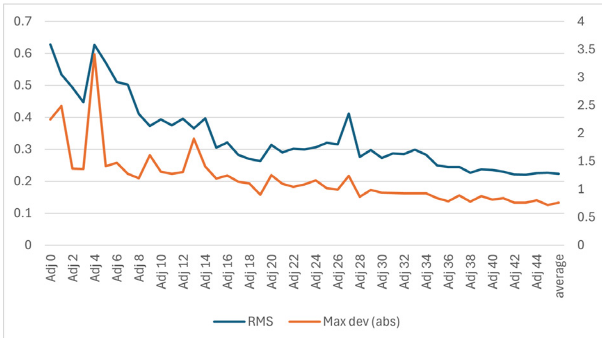

Fig. 4: RMS evolution for d-pillar

The maximum absolute deviation decreases more slowly. It is reduced from 2.27 mm for the datum-only configuration to 0.72 mm after 45 iterations. The strict stopping threshold of 0.05 mm is not reached within 50 iterations; convergence is instead assessed using the plateau criterion defined in Section 3.5. For the present case this occurs well before the iteration limit is reached, and the final configuration represents a balanced compromise between reconstruction accuracy and the number of constraint nodes.

Table 1 summarizes the error metrics for the initial datum-only configuration and for the final configuration obtained with the two-neighbor setting. The results show that the RMS error is reduced to roughly one third of its initial value, and the maximum deviation is reduced significantly.

Table 1: Reconstruction accuracy for the d-pillar.

Configuration	#constraint nodes	RMS [mm]	Max dev. [mm]
Datum only	0	0.628	2.271
Final (greedy)	135	0.224	0.720

5.2. Spatial distribution of selected constraint nodes

The spatial distribution of the selected constraint nodes reflects the deformation behavior of the d-pillar. In addition to the locating features, constraint nodes are primarily added in regions exhibiting pronounced form deviations. Stiffer areas and regions close to the datum features generally require fewer additional constraints. The filtering strategy places constraint nodes away from sharp edges and radii.

5.3. Comparison with alternative neighbor settings

All configurations show a rapid decrease in RMS when the first constraint nodes are added, followed by diminishing returns. Increasing the number of neighbors per iteration leads to a somewhat lower final RMS, but at the cost of a substantially larger total number of constraint nodes.

Quantitatively, the RMS decreases from 0.224 mm for the 2-neighbor setting to 0.221 mm and 0.217 mm for the 3- and 4-neighbor settings, respectively. The corresponding numbers of constraint nodes increase from 141 to 186 and 231. The results indicate that moving from two to three or four neighbors per iteration yields only a modest additional reduction in RMS, while the number of constraint nodes increases noticeably. Given typical levels of measurement noise and modeling uncertainty, the additional reduction in RMS may be of limited practical value relative to the increased model size.

These results support the preliminary stability finding: increasing neighbors increases the constrained local area, but beyond a small patch the benefit becomes marginal compared with the added model size.

5.4. Reconstruction behaviour for the fender

For the fender, the datum-only reconstruction results in an RMS deviation of approximately 1.70 mm with a corresponding maximum absolute deviation of 4.88 mm.

The greedy algorithm is applied using the same two-neighbor setting as for the d-pillar (i.e., activation of the peak-error node plus two neighboring nodes per iteration), the set of constraint nodes is gradually expanded over successive iterations. As additional constraints are introduced, the RMS deviation decreases overall, although convergence is slower than for the d-pillar.

After 50 iterations, a total of 150 additional constraint nodes have been activated. The RMS evolution exhibits noticeable iteration-to-iteration fluctuations. To reduce the influence of these fluctuations, the final reconstruction accuracy is evaluated as the average RMS over the last three iterations, yielding a final RMS value of approximately 0.53 mm. The corresponding iterative reconstruction required approximately 2 h of wall-clock time.

Figure 5 shows the RMS deviation as a function of iteration number for the fender case. Compared with the datum-only configuration, a clear reduction in RMS is observed, with convergence assessed using the plateau criterion defined in Section 3.5.

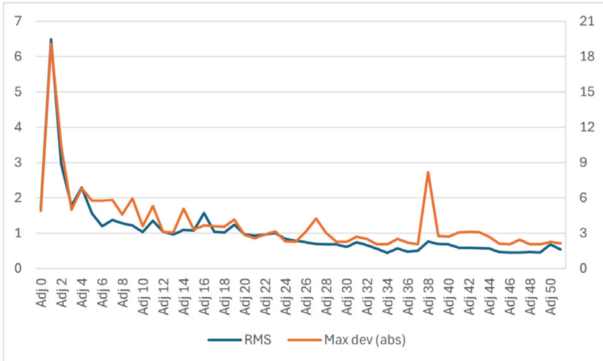

Fig. 5: RMS evolution for fender

The maximum absolute deviation is reduced from 4.88 mm in the datum-only configuration to 2.24 mm in the final configuration. As for the D-pillar, the predefined stopping threshold on the maximum deviation is not reached within the iteration limit, and convergence is therefore assessed using the plateau criterion defined in Section 3.5.

Table 2 summarizes the reconstruction results for the fender, including both RMS and maximum absolute deviation for the datum-only and final configurations.

Table 2: Reconstruction accuracy for the fender.

Configuration	#constraint nodes	RMS [mm]	Max dev. [mm]
Datum only	0	1.70	4.88
Final (greedy)	150	0.532	2.24

6. Discussion

The results demonstrate that the proposed reconstruction approach is robust across parts with fundamentally different stiffness regimes, from compact structural components to large, compliant exterior panels. In both cases, the datum-only configuration leads to large reconstruction errors, while successive activation of additional constraint nodes reduces the RMS deviation with convergence assessed using the plateau criterion defined in Section 3.5. At the same time, systematic differences are observed between the d-pillar and the fender with respect to convergence rate and final accuracy. The d-pillar converges more rapidly and reaches a lower final RMS level, whereas the fender requires a larger number of iterations and stabilises at a higher RMS value.This confirms that the reconstruction accuracy is governed largely by the mechanical behavior of the part rather than the algorithm parameters.

It should be noted that the two components differ substantially in mesh resolution. The fender model consists of approximately 58 900 nodes, whereas the D-pillar model contains approximately 15 000 nodes. As the reconstruction error metrics are evaluated over all mesh nodes, this difference in discretisation density provides important context when comparing absolute RMS and maximum deviation values between the two cases. For this reason, the comparative assessment focuses primarily on convergence behaviour and relative trends rather than on direct numerical equivalence of error magnitudes.

For early-phase variation simulation, the primary objective is typically to capture the dominant deformation patterns and relative sensitivity of the design, thereby supporting robust concept, locator, and tolerance decisions before physical parts are available, rather than to achieve final inspection-level accuracy [4, 13].

The spatial clustering of selected constraint nodes around dominant deformation regions mirrors findings from PCA-based variation studies, which show that low-stiffness areas contribute disproportionately to global shape variability [14]. For the d-pillar, constraint nodes concentrate in local flexible regions, whereas the fender requires more widely spread constraint nodes due to global deformation behavior. This suggests that the algorithm not only improves reconstruction accuracy but also implicitly identifies stiffness-critical locations.

From an industrial geometry-assurance perspective, the method enables the construction of reduced models suitable for large-scale Monte Carlo simulation at the concept stage in tools such as RD&T, when dense measurement data are not yet available. The ability to scale the method across different part types is critical for practical adoption.

Several methodological limitations remain. Measurement noise and alignment uncertainty introduce fluctuations late in the iteration sequence, motivating the averaging strategy. Extending the method to incorporate richer inspection modalities, such as region-specific scan paths or adaptive point distributions, would build upon recent advances in inspection-path optimisation [3].

7. Conclusion

This paper presented a method for predicting sheet-metal part form from sparse metrology information using a compliant FE model and an adaptive constraint node selection algorithm. The approach was evaluated on two geometrically distinct BIW components: a compact d-pillar and a large front fender. In both cases the method substantially reduced the reconstruction error relative to a datum-only baseline, achieving final RMS values of approximately 0.22 mm and 0.53 mm, respectively.

The results demonstrate that the approach generalises across different stiffness regimes and is capable of capturing both local and global deformation modes with a limited number of constraint nodes. This makes the reduced models suitable for early-phase variation simulation, where dense measurement data are not yet available but credible deformation representation is required.

The ability to reconstruct physically plausible deformation fields from sparse inspection data aligns with the needs of digital-twin concepts, which depend on rapid and reliable geometry predictions upstream of assembly operations [15].

Future work will address improved noise robustness, integration with material-and forming-induced variation models, and extension toward assembly-level non-rigid variation prediction.

Acknowledgements

This work was carried out at the Wingquist Laboratory within the Area of Advance Production at Chalmers University of Technology and supported by Sweden's Innovation Agency (VINNOVA). The support of the project DigiSync (grant ID 2024-02505) is gratefully acknowledged.

References

[1] S. H. S.C. Liu, Variation simulation for deformable sheet metal assemblies using finite element methods, Journal of Manufacturing Science and Engineering (ASME) 119 (3) (1997) 368–374. doi:10.1115/1.2831115.

[2] K. Wärmefjord, R. Söderberg, L. Lindkvist, A measure of the information loss for inspection point reduction, Journal of Manufacturing Science and Engineering 131 (5) (2009) 051011. doi:10.1115/DETC2008-49708.

[3] Y. Cao, Z. Huang, K. Guo, L. Qiao, A description method of in-plane geometric deviation of parts based on scanning toolpath deviation coordinate system, Procedia CIRP 114 (2022) 106–111. doi:10.1016/j.procir.2022.10.015.

[4] R. Söderberg, K. Wärmefjord, L. Lindkvist, J. S. Carlson, Virtual geometry assurance process and toolbox, Procedia CIRP 43 (2016) 3–12. doi:10.1016/j.procir.2016.02.043.

[5] J. Dantan, L. Homri, Overview of mathematical concepts for tolerance analysis, Procedia CIRP 129 (2024) 73–78. doi:10.1016/j.procir.2024.10.014.

[6] N. Anwer, A. Ballu, L. Mathieu, The skin model, a comprehensive geometric model for engineering design, CIRP Annals – Manufacturing Technology 62 (1) (2013) 143–146. doi:10.1016/j.cirp.2013.03.078.

[7] B. Schleich, N. Anwer, L. Mathieu, S. Wartzack, Skin model shapes: A new paradigm shift for geometric variations modelling in mechanical engineering, Computer-Aided Design 50 (2014) 1–15. doi:10.1016/j.cad.2014.01.001.

[8] W. Qie, M. Balaghi, N. Anwer, Q. Zhu, Wasserstein generative adversarial networks for form defects modeling, Procedia CIRP 114 (2022) 7–12. doi:10.1016/j.procir.2022.10.002.

[9] E. Morse, C. Grohol, Practical conformance evaluation in the measurement of flexible parts, CIRP Annals 68 (1) (2019) 507–510. doi:10.1016/j.cirp.2019.04.076.

[10] B. Lindau, K. Wärmefjord, L. Lindkvist, R. Söderberg, Virtual fixturing: Inspection of a non-rigid detail resting on 3-points to estimate free state and over-constrained shapes Volume 2B: Advanced Manufacturing (2020) V02BT02A065. doi:10.1115/IMECE2020-24515.

[11] F. Wagersten, Non-rigid variation simulation and geometry assurance for sheet metal assemblies, Ph.D. thesis, Chalmers University of Technology (2010).

[12] A. Rezaei Aderiani, K. Wärmefjord, R. Söderberg, L. Lindkvist, B. Lindau, Optimal design of fixture layouts for compliant sheet metal assemblies, The International Journal of Advanced Manufacturing Technology 110 (7–8) (2020) 2181–2201. doi:10.1007/s00170-020-05954-y.

[13] A. Das, P. Franciosa, D. Williams, D. Ceglarek, Physics-driven shape variation modelling at early design stage, Procedia CIRP 41 (2016) 1072–1077. doi:10.1016/j.procir.2016.01.031.

[14] B. Lindau, L. Lindkvist, A. Andersson, R. Söderberg, Statistical shape modeling in virtual assembly using pca-technique, Journal of Manufacturing Systems 32 (3) (2013) 456–463.

[15] R. Söderberg, K. Wärmefjord, J. S. Carlson, L. Lindkvist, Toward a digital twin for real-time geometry assurance in individualized production, CIRP Annals 66 (1) (2017) 137–140. doi:10.1016/j.cirp.2017.04.038.